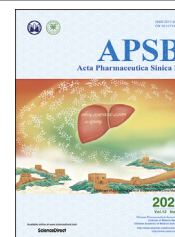




Chinese Pharmaceutical Association
Institute of Materia Medica, Chinese Academy of Medical Sciences

Acta Pharmaceutica Sinica B

www.elsevier.com/locate/apsb
www.sciencedirect.com



ORIGINAL ARTICLE

Spatio-temporal delivery of both intra- and extracellular toll-like receptor agonists for enhancing antigen-specific immune responses



Nannan Wang[†], Yueyue Zuo[†], Shengjie Wu, Chenlu Huang,
Linhua Zhang^{*}, Dunwan Zhu^{*}

Tianjin Key Laboratory of Biomedical Materials, Key Laboratory of Biomaterials and Nanotechnology for Cancer Immunotherapy, Institute of Biomedical Engineering, Chinese Academy of Medical Sciences & Peking Union Medical College, Tianjin 300192, China

Received 11 February 2022; received in revised form 25 April 2022; accepted 10 May 2022

KEY WORDS

Lipid-polymer hybrid nanoparticles;
TLR agonist combinations;
Ovalbumin;
Monophosphoryl lipid A;
Imiquimod;
Nanovaccine;
Spatio-temporal manner;
Cancer immunotherapy

Abstract For cancer immunotherapy, triggering toll-like receptors (TLRs) in dendritic cells (DCs) can potentiate antigen-based immune responses. Nevertheless, to generate robust and long-lived immune responses, a well-designed nanovaccine should consider different locations of TLRs on DCs and co-deliver both antigens and TLR agonist combinations to synergistically induce optimal antitumor immunity. Herein, we fabricated lipid-polymer hybrid nanoparticles (LPNPs) to spatio-temporally deliver model antigen ovalbumin (OVA) on the surface of the lipid layer, TLR4 agonist monophosphoryl lipid A (MPLA) within the lipid layer, and TLR7 agonist imiquimod (IMQ) in the polymer core to synergistically activate DCs by both extra- and intra-cellular TLRs for enhancing adaptive immune responses. LPNPs-based nanovaccines exhibited a narrow size distribution at the mean diameter of 133.23 nm and zeta potential of -2.36 mV, showed a high OVA loading (around 70.83 $\mu\text{g}/\text{mg}$) and IMQ encapsulation efficiency (88.04%). Our data revealed that LPNPs-based nanovaccines showed great biocompatibility to immune cells and an excellent ability to enhance antigen internalization, thereby promoting DCs maturation and cytokines production. Compared to Free OVA, OVA-LPNPs promoted antigen uptake, lysosome escape, depot effect and migration to secondary lymphatic organs. *In vivo* immunization showed that IMQ-MPLA-OVA-LPNPs with dual agonists induced more powerful cellular and humoral immune responses. Moreover, prophylactic vaccination by IMQ-MPLA-OVA-LPNPs effectively suppressed tumor growth

^{*}Corresponding authors. Tel./fax: +86 22 87891191.

E-mail addresses: zhanglinhua@bme.pumc.edu.cn (Linhua Zhang), zhudunwan@bme.pumc.edu.cn (Dunwan Zhu).

[†]These authors made equal contributions to this work.

Peer review under the responsibility of Chinese Pharmaceutical Association and Institute of Materia Medica, Chinese Academy of Medical Sciences

<https://doi.org/10.1016/j.apsb.2022.05.032>

2211-3835 © 2022 Chinese Pharmaceutical Association and Institute of Materia Medica, Chinese Academy of Medical Sciences. Production and hosting by Elsevier B.V. This is an open access article under the CC BY-NC-ND license (<http://creativecommons.org/licenses/by-nc-nd/4.0/>).

and increased survival efficacy. Hence, the nanovaccines we fabricated can effectively co-deliver antigens and different TLR agonists and realize coordinated stimulation of DCs in a spatio-temporal manner for enhanced immune responses, which provides a promising strategy for cancer immunotherapy.

© 2022 Chinese Pharmaceutical Association and Institute of Materia Medica, Chinese Academy of Medical Sciences. Production and hosting by Elsevier B.V. This is an open access article under the CC BY-NC-ND license (<http://creativecommons.org/licenses/by-nc-nd/4.0/>).

1. Introduction

Cancer poses a serious threat to human life and health. There are about 24.5 million cancer cases and 9.6 million deaths worldwide every year^{1–3}. However, the results of cancer treatment are still not optimistic enough, mainly because tumors can induce immunosuppression by blocking the immune system from recognizing tumor-associated antigens (TAAs), or by actively suppressing immune effector cells to prevent them from killing tumor cells⁴. In recent years, immunotherapy has emerged as a novel and promising strategy, showing distinct advantages over traditional cancer treatment paradigms (chemotherapy and radiotherapy) including reduced side effects, increased specificity and long-term anti-tumor responses. Immunotherapy aims at activating anti-tumor immunity by training the body's immune system to correctly recognize antigen specificity and promoting the proliferation and function of effector cells⁵. Professional antigen-presenting cells (APCs), especially dendritic cells (DCs), play a vital role in this process⁶. DCs are the bridge between innate and adaptive immune responses⁷. After the antigen being captured and processed, the DCs present antigen-associated peptide to T cells to elicit CD8⁺ cytotoxic T lymphocyte (CTL) responses *via* MHC-I molecules or to activate CD4⁺ T cells-mediated humoral immunity *via* MHC-II molecules^{6,8}. Therefore, the key to the success of immunotherapy is how to most effectively regulate DCs to induce desired immune responses.

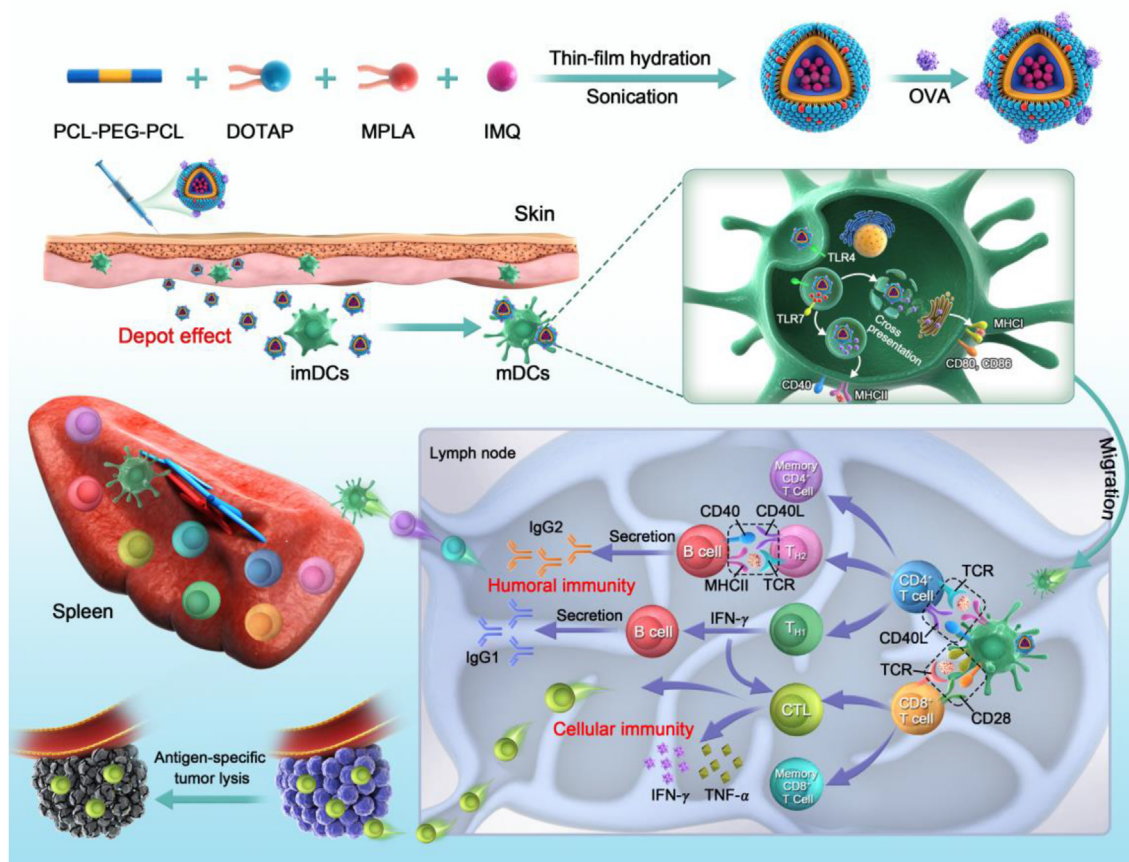
Nanoparticles have many benefits that make them appropriate for eliciting immune responses by delivering payloads to DCs and improving the efficacy of cancer immunotherapy^{9–14}. For example, nanoparticle vaccine delivery systems provide the ability to protect the loaded bioactive molecules, allow co-encapsulation of antigens and multiple adjuvants, control their delivery and function in a spatio-temporal manner, and engineer DCs for potent T cell activation^{15,16}. Among them, liposomes and polymeric nanoparticles have been widely studied as potential vaccine platforms^{17,18}. Nevertheless, liposomes have several limitations such as lack of structural integrity, insufficient drug loading and fast drug leakage. Polymeric nanoparticles suffer from lower biocompatibility and insufficient encapsulation of hydrophilic drugs. To overcome the disadvantages of liposomes and polymeric nanoparticles, lipid-polymer hybrid nanoparticles (LPNPs) have emerged as an innovative nanoparticle delivery system, which is formed by a polymer core enveloped with a single- or multiple-lipid layer. LPNPs not only exhibit high stability and biocompatibility, but also show improved encapsulation and reduced leakage of drugs. Furthermore, LPNPs have a latent capacity as a vaccine delivery system due to that their structures are similar to viral architecture¹⁹.

Delivery of vaccine to DCs can be accomplished in many diverse ways, in which antigens and immunostimulants encapsulated within the same nanoparticles have demonstrated successful antigen (cross-) presentation and CTL responses, leading to

improved immunotherapeutic efficacy^{20–22}. For example, Wilson et al.²³ formulated a pH-responsive nanoparticle vaccine for co-delivery of ovalbumin (OVA) antigen and toll-like receptor (TLR) agonist, which significantly enhanced the antigen-specific CD4⁺ and CD8⁺ T cell responses. Recent studies revealed that combined activation of immune cells *via* different TLR agonists could further augment the antigen-specific immune responses. Kasturi et al.²⁴ confirmed that the combination of two TLR agonists with different signaling mechanisms enhanced antigen-specific T cell responses and the production of neutralizing antibodies compared to a single TLR ligand. Signaling *via* TLR7 depends on the adapter molecule myeloid differentiation primary-response gene 88 (MYD88), while signaling *via* TLR4 involves both MYD88 and Toll/IL-1R (TIR)-domain-containing adapter protein inducing interferon- β (TRIF) pathways²⁵. Therefore, the combination of TLR4 and TLR7 agonists is likely to mediate a stronger immune response.

Monophosphoryl lipid A (MPLA), an agonist of TLR4, can induce a strong Th1-biased immune response while significantly reducing the toxicity of LPS to 100–10,000 times^{26–29}. MPLA has been successfully employed in several commercial vaccines in the treatment of cervical cancer (Cervarix®), hepatitis (Fendrix®), and malaria (RTS, S®)³⁰. Imiquimod (IMQ), an agonist of TLR7, is a promising DCs activator and has been approved by FDA as an immunomodulatory agent^{30,31}. Topical administration of IMQ has shown effectiveness in the treatment of several skin diseases. Aldara® (IMQ 5% cream) has been approved for the treatment of external genital warts, actinic keratosis, and superficial basal cell carcinoma³². TLR4 locates both on the cell membrane and in the endosomes, while TLR7 is an endosomal receptor. Studies demonstrated that the cellular location of TLRs can strongly influence the TLR ligand accessibility and regulate the subsequent immune response^{33,34}. Thus, appropriate TLR agonists selection and rational design of particulate vaccine are critically important to precisely control the immune responses and achieve better immunotherapeutic effects.

In this work, we sought to develop a novel versatile LPNPs nanovaccine system (IMQ-MPLA-OVA-LPNPs) to co-deliver antigen and synergistic TLR agonists to the same DCs in a spatio-temporal manner for enhancing antigen-specific immune responses (Scheme 1). FDA-approved biodegradable polymers poly(ϵ -caprolactone) (PCL) and poly(ethylene glycol) (PEG) were used to construct the inner polymer core of LPNPs, while 1,2-dioleoyl-3-trimethylammonium-propane (DOTAP) which has been proved to promote antigen uptake, lysosomal escape, and DC maturation was used as the lipid layer to decorate on the outer surface of the inner polymer core³⁵. Considering the locations of TLR4 and TLR7 on DCs, TLR7 agonist IMQ was incorporated into the hydrophobic polymer core of the LPNPs, while TLR4 agonist MPLA was decorated within the outer lipid layer. At the same time, the OVA model antigen was adsorbed by the positive DOTAP and dispersed on the outer layer of the LPNPs. After



Scheme 1 Schematics of the preparation of OVA-loaded DOTAP-LPNPs with dual agonists and proposed mechanisms in cancer immunotherapy.

immunization, the MPLA on the LPNPs' surface would bind with extracellular TLR4, thus enhancing the uptake of LPNPs nanovaccines by DCs. Then, the DOTAP facilitated antigen escape and cross-presentation *via* its "sponge effect". In addition, the released IMQ would ligate with endosome-associated TLR7. The synergistic stimulation of DCs by extracellular TLR4 and intracellular TLR7 signaling pathway can induce powerful cellular and humoral immune responses, thus achieving better prophylactic vaccination efficacy against EG7-OVA tumor model. The LPNPs-based nanovaccines can spatio-temporally deliver intra- and extracellular TLR agonists to enhance antigen-specific immune responses, holding great promise to be developed as rational and versatile vaccines for effective cancer immunotherapy.

2. Materials and methods

2.1. Materials

PCL-PEG-PCL triblock copolymer was synthesized according to our previous literature^{36,37}. DOTAP, rhodamine-PE, and MPLA were obtained from Avanti Polar Lipids (Alabaster, AL, USA). OVA and FITC were purchased from Sigma-Aldrich (St. Louis, MO, USA). IMQ was obtained from Tokyo Chemical Industry Company (St. Louis, MO, USA). Recombinant murine TNF- α , IL-4, and GM-CSF were obtained from Peprotech (Rocky Hill, NJ, USA). Fluorochrome-labeled CD11c, CD3, CD8, CD4, CD86, CD80, CD40, CD69, CD44, and CD62L antibodies were purchased from eBioscience (San Diego, CA, USA). Pierce™ BCA

protein assay kit was obtained from Thermo Fisher Scientific (Waltham, MA, USA). DAPI and Lyso Tracker-Red DND-99 were acquired from Beyotime Biotechnology (Shanghai, China). Female C57BL/6 mice were acquired from Beijing Vital River Laboratory Animal Technology Co., Ltd. (Beijing, China). All animals were treated according to the protocol approved by Chinese Academy of Medical Science and Peking Union Medical College.

2.2. Preparation and characterization of LPNPs-based nanovaccines

DOTAP cationic lipid-polymer hybrid nanoparticles (DOTAP-LPNPs) were formulated using thin-film rehydration method³⁸. Briefly, PCL-PEG-PCL copolymer (20 mg) and DOTAP (1 mg) were dissolved in dichloromethane (DCM). Then, DCM was totally evaporated to obtain a thin-film layer. After hydrating the thin-film with 5 mL of ultra-pure water (65 °C, 5 h), the dispersion was sonicated by a VCX-130-PB microtip probe sonicator (Sonics & Material Inc., Newtown, CT, USA) for 10 min. The resulted DOTAP-LPNPs dispersion was mixed with OVA solution (1 mg/mL, 1.5 mL) at 4 °C to form OVA-loaded DOTAP-LPNPs. OVA-loaded DOTAP-LPNPs containing IMQ and/or MPLA were prepared by additional adding IMQ (100 μ g) and/or MPLA (10 μ g) in DCM with the copolymer and DOTAP and then prepared as described above.

The morphology of the DOTAP-LPNPs was observed by transmission electron microscope (TEM, FEI Co., Eindhoven,

Netherlands). To directly observe the lipid layer, larger DOTAP-LPNPs with rhodamine-PE-labeled lipid layer were formulated by additional adding 0.2% rhodamine-PE and sonicating only 1 min instead of 10 min. After that, confocal laser scanning microscope (CLSM710, Carl ZEISS, Jena, Germany) was used to observe the obtained DOTAP-LPNPs. The particle size and zeta potential of the various LPNPs-based nanovaccines were measured *via* a NanoZS Zetasizer (Malvern Instruments Ltd., Worcestershire, UK).

To determine the OVA loading content (LC) and encapsulation efficiency (EE), Pierce™ BCA Protein Assay Kit was utilized to evaluate the amounts of unbound OVA in supernatant. The LC and EE were determined as Eqs. (1) and (2), respectively:

$$\text{LC (\%)} = (\text{Total protein} - \text{Unadsorbed protein}) / \text{Total dry weight of nanovaccines} \times 100 \quad (1)$$

$$\text{EE (\%)} = (\text{Total protein} - \text{Unadsorbed protein}) / \text{Total protein} \times 100 \quad (2)$$

To study the *in vitro* OVA release, OVA-loaded DOTAP-LPNPs dispersion was put in a dialysis bag and kept shaking in pH 7.4 PBS solution at 37 °C. The whole PBS solution was removed and replaced with fresh PBS at the predetermined time. The amounts of OVA released in the PBS solution were measured using BCA assay.

To evaluate the LC and EE of IMQ, the lyophilized IMQ-loaded LPNPs were dissolved in DMSO and then measured by UV–Vis spectrophotometer (Lambda35, PerkinElmer, Waltham, MA, USA) at 325 nm. The LC and EE were calculated according to Eqs. (3) and (4), respectively:

$$\text{LC (\%)} = (\text{Amount of loaded drug} / \text{Amount of LPNPs}) \times 100 \quad (3)$$

$$\text{EE (\%)} = (\text{Amount of loaded drug} / \text{Amount of feeding drug}) \times 100 \quad (4)$$

To study the IMQ release, IMQ-loaded LPNPs were dialyzed against PBS solution (pH 7.4 and 5.5) as described above. IMQ released in the PBS solution was extracted with DCM twice and then dissolved in DMSO after DCM was evaporated. Following that, the absorbance of IMQ solution was measured at 325 nm using UV–Vis spectrophotometer (PerkinElmer).

2.3. *In vitro* DCs maturation

Bone marrow dendritic cells (BMDCs) were isolated and cultured as previously described³⁹. Then, the obtained immature DCs were cultured with Free OVA or various OVA-loaded DOTAP-LPNPs for 24 h. Afterwards, the DCs were collected to stain with PerCP-Cy5.5-anti CD11c, APC-anti CD80, FITC-anti CD86 and PE-anti CD40, and then analyzed by flow cytometry (BD FACSCalibur, Franklin Lake, NJ, USA).

2.4. *In vitro* cytotoxicity of LPNPs-based nanovaccines

DCs viability following different treatments was measured using MTS assay. Briefly, BMDCs (1×10^5 cells/well) were cultured in 96-well plates overnight, and then incubated with various LPNPs-based nanovaccines at OVA concentrations ranged from 6.25 to

100 µg/mL for 24 h. Afterwards, MTS reagent was added into each well and incubated at 37 °C for 2 h. Finally, the absorbance at 490 nm was determined by a Thermo Scientific microplate reader (Thermo Varioskan Flash3001, Waltham, MA, USA).

2.5. Antigen uptake and intracellular localization in BMDCs

Immature BMDCs were cultivated with OVA-FITC or LPNPs-based OVA-FITC nanovaccines (equivalent 10 µg/mL OVA) for 16 h at 37 °C. After washing with PBS (10 mmol/L, pH 7.4), the cells were stained with anti-CD11c antibody solution to identify DCs. The percentage of CD11c⁺ OVA-FITC⁺ cells was determined using a BD FACSCalibur.

To further determine antigen intracellular localization and lysosomal escape, immature BMDCs were cultivated with Free OVA-FITC or various LPNPs-based OVA-FITC nanovaccines (16 h, 37 °C). Then, the cells were washed thrice to remove the spare OVA-FITC. Next, the cells were stained with Lyso Tracker Red DND-99 to visualize late endosomes and lysosomes as well as labeled with DAPI to visualize the nucleus. Finally, CLSM (Carl ZEISS) was used to record the fluorescent images. The co-localization level of OVA-FITC and lysotracker was calculated by Zeiss LSM software (Carl ZEISS, Jena, Germany).

2.6. *In vivo* tracking of LPNPs-based nanovaccines

Female C57BL/6 mice were subcutaneously administered with rhodamine-labeled OVA or various LPNPs-based OVA-rhodamine nanovaccines on their tail base. The *in situ* fluorescent signals at draining lymph nodes (LNs) and injection sites were detected by CRI Maestro imaging system (CRI, MA, USA) (filter sets: λ_{ex} , 560 nm; λ_{em} , 600 nm). 6 days after injection, inguinal LNs were isolated to acquire *ex vivo* fluorescence images. The acquired images were further analyzed by CRI Maestro software (MA, USA).

2.7. *In vivo* activation of DCs on draining LNs

Female C57BL/6 mice were subcutaneously administered with PBS, Free OVA or various LPNPs-based nanovaccines at OVA dose of 25 µg per mouse. On Day 7, the inguinal LNs were cut out and triturated into cell suspension. After staining with PerCP-Cy5.5-anti-CD11c, FITC-anti-CD86, PE-anti-CD40, APC-anti-MHC I, FITC-anti-MHC II, the cells were detected by FACS (BD) to assess the surface markers on DCs.

2.8. *In vivo* immunization studies

Female C57BL/6 mice were immunized with PBS, Free OVA or various LPNPs-based nanovaccines including OVA-LPNPs, MPLA-OVA-LPNPs, IMQ-OVA-LPNPs, and IMQ-MPLA-OVA-LPNPs by subcutaneous injection on Day 0 and Day 14 (25 µg OVA/mouse). Blood was collected on Days 0 (prior to the priming vaccination), 7, 14 (prior to boosting) and 21 for analysis of OVA-specific IgG and IgG isotypes (IgG2a and IgG1) using ELISA kits. 7 days after boost immunization, splenocytes were obtained and re-stimulated with 50 µg/mL Free OVA for 72 h in a 24-well plate. Then, the supernatants were collected to analyze the production of IFN- γ and TNF- α by ELISA kits. After washing, the splenocytes were labeled with FITC-anti-CD3e, APC-anti-CD4, PE-anti-CD8, FITC-anti-CD19, PerCP-Cy5.5-anti-CD69, FITC-anti-CD44, PerCP-Cy5.5-anti-CD62L and APC-labeled SIINFEKL/H-2Kb pentamer for FACS (BD) measurement.

2.9. *In vivo* tumor challenge

To assess the prophylactic effect, C57BL/6 mice were randomly separated into 5 groups ($n = 8$) and vaccinated twice as described above. Seven days post the 2nd vaccination, 1×10^6 EG7-OVA cells were subcutaneously administered into the right flank of the mice. Tumor size was monitored over time by an electronic digital caliper (GUANGLU, ARZ-1331, Guilin, China). Tumor volume was determined by the following formula: length \times width²/2. For the survival study, the mice were considered dead when the tumor length was greater than 20 mm.

2.10. Statistical analysis

Data were presented as mean \pm standard deviation. Statistical differences were assessed using One-way ANOVA method. Statistical significance was considered when P -value < 0.05 .

3. Results and discussion

3.1. Preparation and characterization of LPNPs-based nanovaccines

OVA-loaded DOTAP-LPNPs containing IMQ and/or MPLA were successfully fabricated using thin-film rehydration method (Scheme 1). The prepared LPNPs comprised three functional assemblies: 1) an inner hydrophobic core for the encapsulation of lipophilic immunostimulant IMQ (TLR7 agonist), 2) an interfacial surface for the attachment of MPLA (TLR4 agonist), and 3) a cationic DOTAP layer for electronic adsorption of model antigen OVA. Fig. 1A showed CLSM images of the DOTAP-LPNPs, where the lipid shells were labeled by rhodamine-PE. The apparently observed red shell demonstrated that a lipid layer was successfully created on the surface of the DOTAP-LPNPs using the above-mentioned preparation method. Meanwhile, TEM images of DOTAP-LPNPs showed a clear lipid shell enveloping on the surface (Fig. 1B), whereas the formulated OVA-loaded DOTAP-LPNPs were spherical in shape with visible particles attached on the NPs (Fig. 1C and D), demonstrating the successful adsorption of OVA antigen *via* cationic DOTAP lipid. The DOTAP-LPNPs had a positive surface charge of around 23 mV. After adsorbing OVA on the cationic layer of the DOTAP-LPNPs *via* electrostatic interactions, the zeta potential changed to a slightly negative charge (around -2 mV), further confirming that OVA was loaded on the surface of the LPNPs. As shown in Fig. 1E, OVA-loaded DOTAP-LPNPs exhibited a narrow size distribution. *In vitro* release study showed that OVA antigen was released rapidly from the OVA-loaded DOTAP-LPNPs, contributing to that OVA was physically adsorbed on the surface of the nanovaccines (Fig. 1F). The LC and EE of IMQ were 0.42% and 88.04%, respectively. As shown in Fig. 1G, IMQ was released in a slow and sustained manner, due to the encapsulation within the inner hydrophobic core of the nanovaccines. In addition, accelerated IMQ release was observed at pH 5.5, ascribing to the protonation of aromatic amines in IMQ at acidic conditions⁴⁰. The enhanced IMQ release at a reduced pH value is favorable for the binding of IMQ with TLR7 at the acidic endosome. Using the above method, a set of OVA-loaded DOTAP-LPNPs containing IMQ and/or MPLA was constructed as nanovaccines. As shown in Table 1, these LPNPs-based nanovaccines showed similar OVA loading content, particle size, and zeta potential. These results

indicated that the lipophilic IMQ encapsulated within the core and/or the MPLA incorporated at the interfacial surface did not substantially change the physicochemical properties of the LPNPs-based nanovaccines.

3.2. The effect of LPNPs-based nanovaccines on cell viability, antigen internalization and DCs activation *in vitro*

First, *in vitro* cytotoxicity of Free OVA as well as various OVA-loaded DOTAP-LPNPs in DCs was evaluated using MTS assay. The results showed that all the formulations at the OVA concentration ranged from 6.25 to 100 $\mu\text{g}/\text{mL}$ and did not affect the survival of DCs, indicating the great biocompatibility of the prepared cationic LPNPs to immune cells (Fig. 2A).

Then, the antigen internalization by DCs, which was the first step to induce specific immune responses, was quantitatively determined by flow cytometry. The data showed that all OVA-loaded DOTAP-LPNPs significantly increased the cellular uptake of OVA-FITC by DCs, demonstrating their great capability of enhancing antigen internalization (Fig. 2B). After uptake, the internalized antigens are processed in the lysosome to activate CD4⁺ T cells *via* MHC class II presentation route or enter into the cytosol to trigger CD8⁺ T cells activation through MHC class I pathway⁴¹. Effective vaccination against cancer often requires activation of CD8⁺ T cells to induce vigorous CTL responses⁴². Thus, the intracellular antigen processing is critically important for triggering effective T cell immune responses. In our study, BMDCs were cultivated with Free OVA-FITC or various OVA-FITC LPNPs and the intracellular OVA localization was observed using confocal microscopy. As shown in Fig. 2C, weak green fluorescence was detected in BMDCs after incubating with Free OVA-FITC for 16 h, indicating poor uptake of soluble OVA by the endo/lysosome pathway. In contrast, the OVA-loaded DOTAP-LPNPs dramatically enhanced green fluorescence in BMDCs, confirming their ability to facilitate cellular uptake of OVA antigen. More importantly, Free OVA-FITC was nearly all overlapped with lysosomes (labeled with Lyso Tracker Red), whereas OVA-FITC from the OVA-loaded DOTAP-LPNPs was observed in both lysosome and cytoplasm. The co-localization of Free OVA, OVA-LPNPs, MPLA-OVA-LPNPs, IMQ-OVA-LPNPs, and IMQ-MPLA-OVA-LPNPs was 79.88%, 62.18%, 55.63%, 59.83%, and 52.28%, respectively, demonstrating that DOTAP-LPNPs facilitated the lysosomal escape of OVA antigen.

After that, the effects of various formulated OVA-loaded DOTAP-LPNPs on BMDCs maturation were evaluated by flow cytometric analysis. As shown in Fig. 3, in comparison to Free OVA, OVA-loaded DOTAP-LPNPs elevated the expression of surface markers by 1.5–5.5-fold. In addition, OVA-loaded DOTAP-LPNPs with immunomodulator IMQ and/or MPLA further elevated the expression of CD40, CD80 and CD86 to different extents compared to the nanovaccines without immunomodulator. More importantly, IMQ-MPLA-OVA-LPNPs with dual immunomodulators induced the highest expression of costimulatory (CD86 and CD80) and adhesion molecules (CD40). The results indicated that OVA-LPNPs with dual TLR agonists can synergistically activate DCs *via* both MPLA engaging with extracellular TLR4 and IMQ binding to intracellular TLR7.

3.3. *In vivo* tracking of OVA-loaded DOTAP-LPNPs

Forming a depot at the vaccination site is essential for the antigen delivery system, which would prolong antigen exposure to the

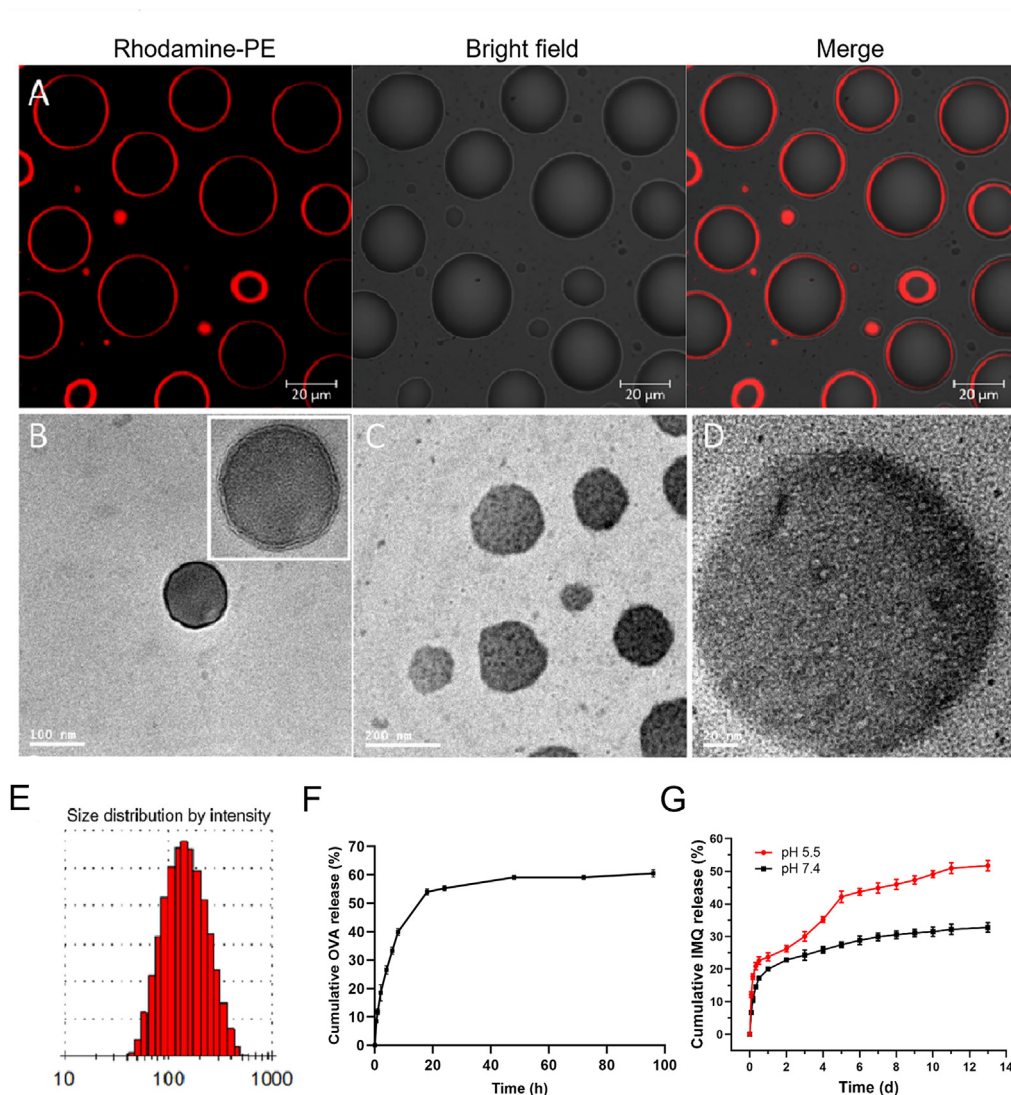
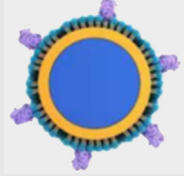
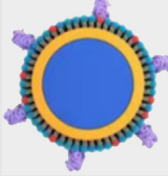
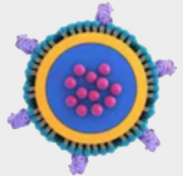
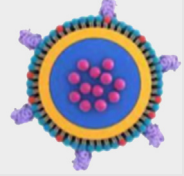


Figure 1 Characterization of OVA-loaded DOTAP-LPNPs. (A) CLSM images of rhodamine-PE labeled large LPNPs (scale bar: 20 μm); (B) TEM micrographs of DOTAP-LPNPs (scale bar: 100 nm); (C) and (D) TEM micrographs of OVA-loaded DOTAP-LPNPs (scale bar: 200 nm (left), 20 nm (right)); (E) Size distribution of OVA-loaded DOTAP-LPNPs; (F) *In vitro* OVA release profile in PBS (pH 7.4) ($n = 3$); (G) *In vitro* IMQ release profile in PBS (pH 7.4 and pH 5.5). Data are presented as mean \pm SD ($n = 3$).

Table 1 Schematic representation and characterization of various OVA-loaded DOTAP-LPNPs ($n = 3$).

Nomenclature	--/OVA	--/MPLA/OVA	IMQ/--/OVA	IMQ/MPLA/OVA
Schematic				
Description	Empty interior, OVA on surface	Empty interior, MPLA coating, OVA on surface	IMQ inside, OVA on surface	IMQ inside, MPLA coating, OVA on surface
Diameter (nm)	139.90 \pm 4.30	133.87 \pm 5.68	146.20 \pm 4.97	133.23 \pm 4.09
Polydispersity index	0.17 \pm 0.02	0.22 \pm 0.02	0.20 \pm 0.01	0.16 \pm 0.01
Zeta potential (mV)	-2.17 \pm 0.51	-2.02 \pm 0.36	-2.74 \pm 0.32	-2.36 \pm 0.40
OVA content ($\mu\text{g}/\text{mg}$)	72.65 \pm 3.79	71.95 \pm 4.12	73.26 \pm 4.68	70.83 \pm 3.64

OVA, ovalbumin; MPLA, monophosphoryl lipid A; IMQ, imiquimod.

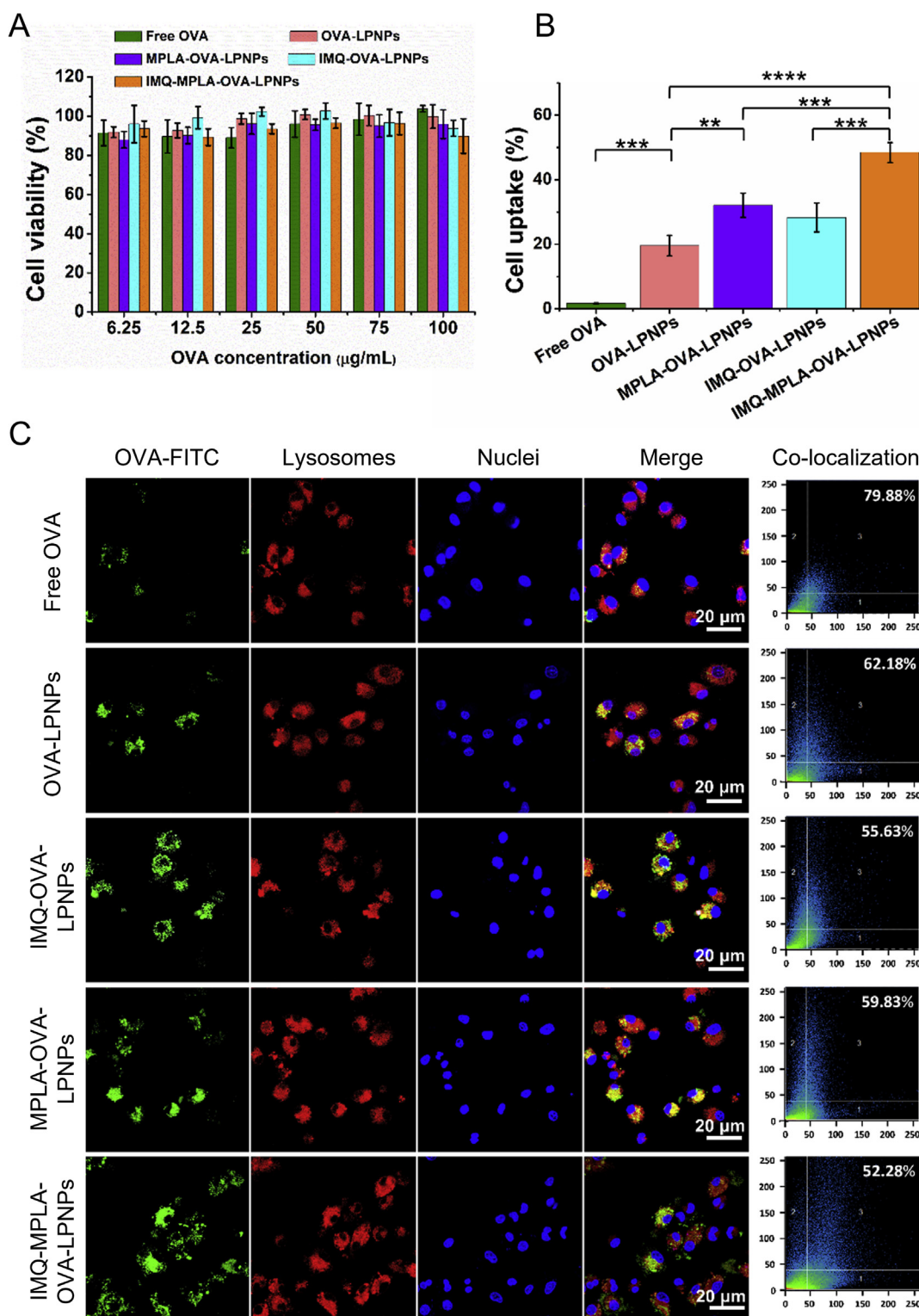


Figure 2 The cytotoxicity, cellular internalization and localization of Free OVA and various OVA-loaded DOTAP-LPNPs in BMDCs. (A) *In vitro* cytotoxicity of BMDCs after cultivating with Free OVA and various OVA-loaded DOTAP-LPNPs for 24 h. Data are presented as mean \pm SD ($n = 3$). (B) Quantification of OVA internalization and (C) intracellular localization in BMDCs after cultivating with Free OVA or various OVA-loaded DOTAP-LPNPs for 16 h. * $P < 0.05$, ** $P < 0.01$, *** $P < 0.001$ and **** $P < 0.0001$ vs. indicated.

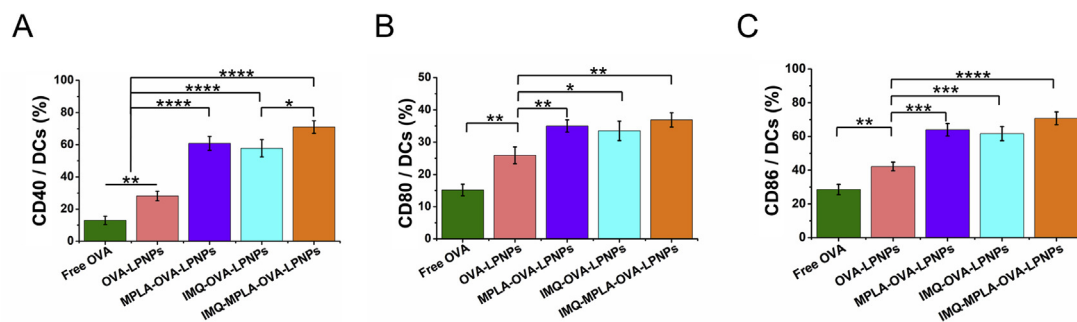


Figure 3 Quantification of CD86⁺, CD80⁺ and CD40⁺ expression on DCs stimulated with Free OVA and various OVA-loaded DOTAP-LPNPs. Data are presented as mean \pm SD ($n = 3$). * $P < 0.05$, ** $P < 0.01$, *** $P < 0.001$ and **** $P < 0.0001$ vs. indicated.

immune system and enhance the antigen capture by the immune cells^{43–45}. Migration of activated DCs to draining LNs is another important factor to initiate adaptive immunity^{46–48}. To evaluate the antigen depot effect and DCs migration, mice were subcutaneously administered with rhodamine-labeled OVA or rhodamine-labeled OVA-loaded DOTAP-LPNPs at the tail base and visualized the fluorescent signal at the injection site and inguinal LNs. As presented in Fig. 4A, the fluorescent signals of the injection sites decreased rapidly and nearly disappeared at 48 h after the injection of Free OVA. However, for OVA-loaded DOTAP-LPNPs, strong fluorescence signals were detected even at 144 h after injection, indicating depot effect of OVA-loaded DOTAP-LPNPs at the injection site. The fluorescence intensity was further quantitatively analyzed by CRI Maestro Analysis software, and the results were coincident with the qualitative results (Fig. 4B). Mice vaccinated with OVA-loaded DOTAP-LPNPs displayed

significantly stronger fluorescence signals in the inguinal draining LNs than those vaccinated with Free OVA at 24 h after injection, suggesting that OVA-loaded DOTAP-LPNPs can efficiently deliver antigen to the LNs (Fig. 4C). Inguinal draining LNs were isolated for *ex vivo* fluorescent imaging 6 days after injection. As shown in Fig. 4D, the OVA-loaded DOTAP-LPNPs group showed a strong fluorescent signal in the draining LNs, while a very weak fluorescent signal was observed for the Free OVA group, further confirming that OVA-loaded DOTAP-LPNPs can enhance accumulation and residence of antigen in the draining LNs.

3.4. *In vivo* activation of DCs by LPNPs-based nanovaccines in draining LNs

After confirming that OVA-loaded DOTAP-LPNPs facilitated DCs migration to the draining LNs, in which naïve T cells are

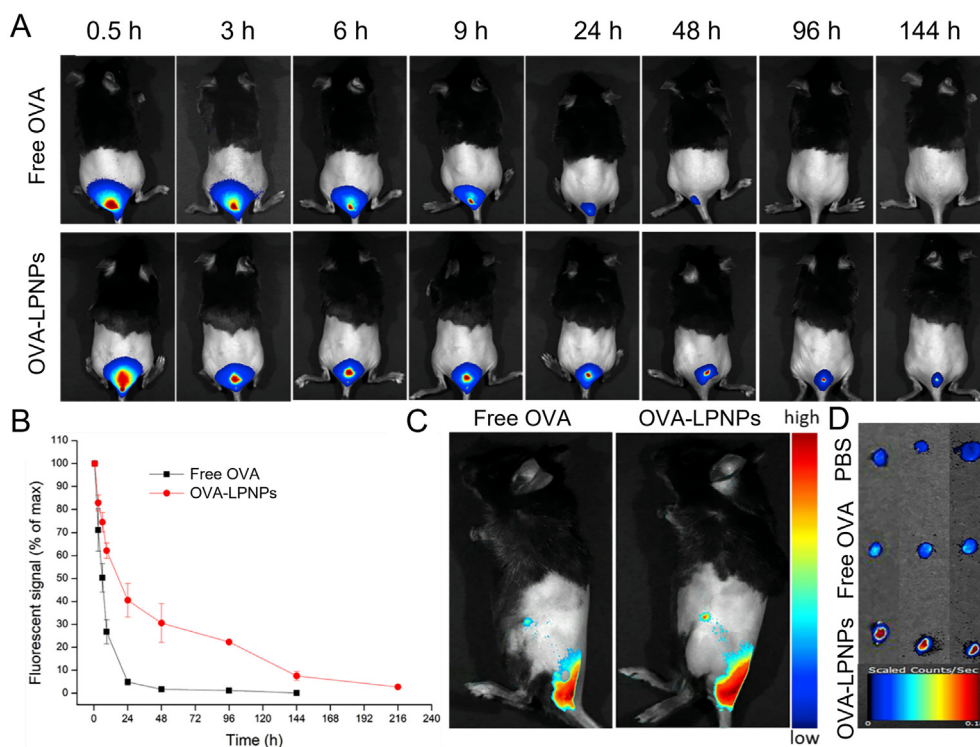


Figure 4 *In vivo* visualization of OVA-loaded DOTAP-LPNPs. (A) NIR fluorescence imaging and (B) quantitative fluorescence intensity of OVA antigen at the tail base ($n = 3$). (C) Representative fluorescence imaging of draining LNs at 24 h after administration of Free OVA or OVA-loaded DOTAP-LPNPs. (D) *Ex vivo* fluorescent image of isolated LNs at 6 days after injection ($n = 3$).

being educated by DCs, the ability of different LPNPs-based nanovaccines in activating DCs there was still unknown. Then, the expression of co-stimulatory molecules (CD86 and CD40) and MHC molecules (MHC I and MHC II) on DCs in the draining LNs were assessed by FACS. As presented in Fig. 5,

LPNPs-based nanovaccines expressed 2.6–3.1-fold higher CD40, 2.1–2.6-fold higher MHC I, and 2.3–3.0-fold higher MHC II than Free OVA. Although OVA-LPNPs and IMQ-OVA-LPNPs slightly elevated CD86 expression in comparison to Free OVA, MPLA-OVA-LPNPs and IMQ-MPLA-OVA-LPNPs

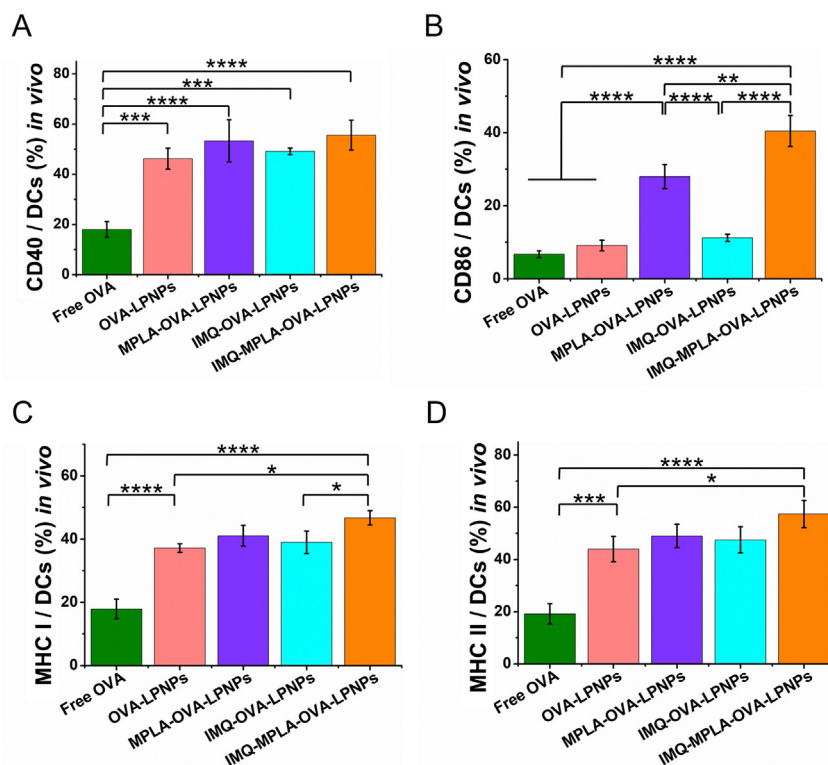


Figure 5 The effects of Free OVA and different LPNPs-based vaccines on DCs activation in draining LNs. The percentages of (A) CD40, (B) CD86, (C) MHC I, and (D) MHC II on CD11c⁺ DCs was quantified by FACS. Data are presented as mean \pm SD ($n = 6$). * $P < 0.05$, ** $P < 0.01$, *** $P < 0.001$ and **** $P < 0.0001$ vs. indicated.

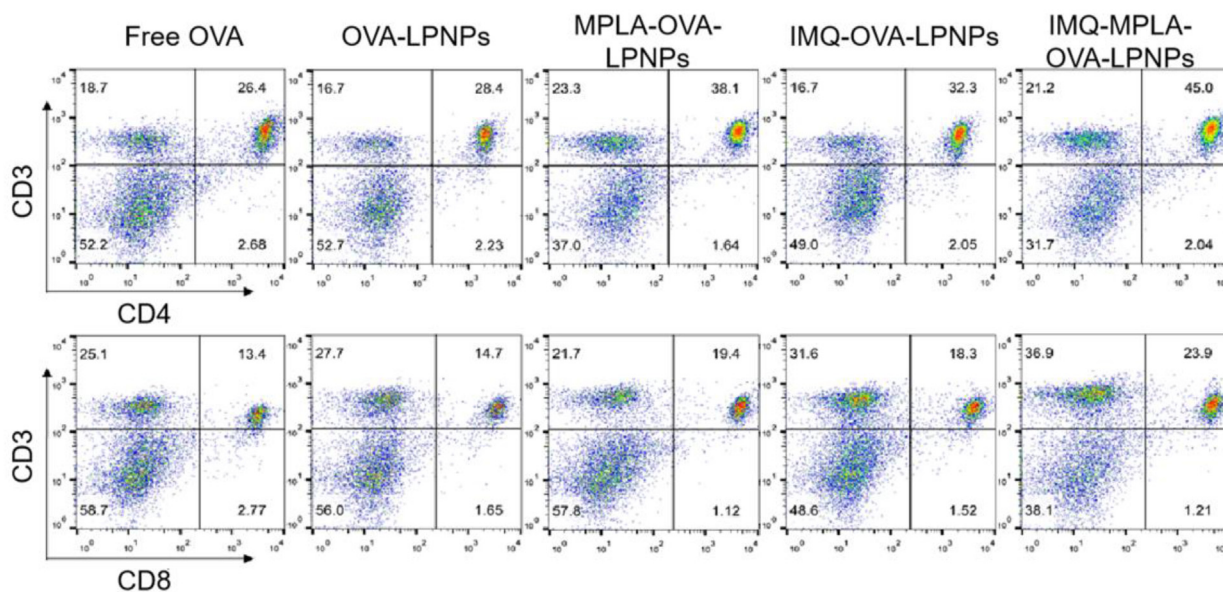


Figure 6 The population and percentage of CD4⁺ and CD8⁺ T cells in splenocytes purified from mice vaccinated with Free OVA or various OVA-loaded DOTAP-LPNPs.

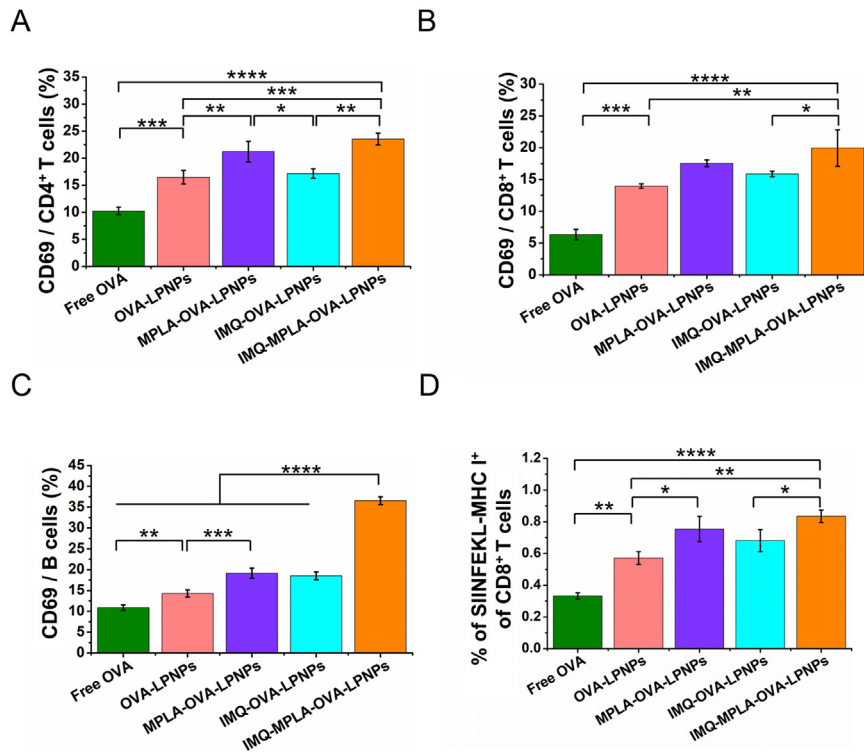


Figure 7 Evaluation of *in vivo* lymphocyte activation. Expression of CD69⁺ on (A) CD4⁺ T cells, (B) CD8⁺ T cells and (C) CD19⁺ B cells evaluated by FACS. (D) Percentage of CD8⁺ SIINFEKL-MHC I⁺ T cells analyzed by FACS. Data are presented as mean \pm SD ($n = 6$). * $P < 0.05$, ** $P < 0.01$, *** $P < 0.001$ and **** $P < 0.0001$ vs. indicated.

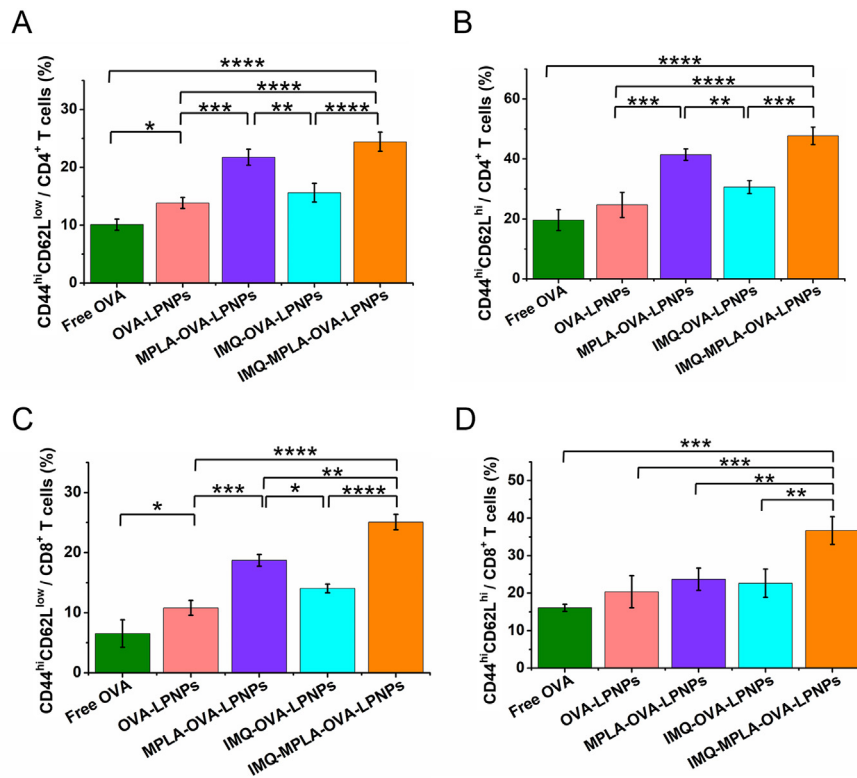


Figure 8 *In vivo* analysis of effector and central memory T cells. (A) T_{EM} and (B) T_{CM} of CD4⁺ cells ($n = 6$). (C) T_{EM} and (D) T_{CM} of CD8⁺ cells. Data are presented as mean \pm SD ($n = 6$). * $P < 0.05$, ** $P < 0.01$, *** $P < 0.001$ and **** $P < 0.0001$ vs. indicated.

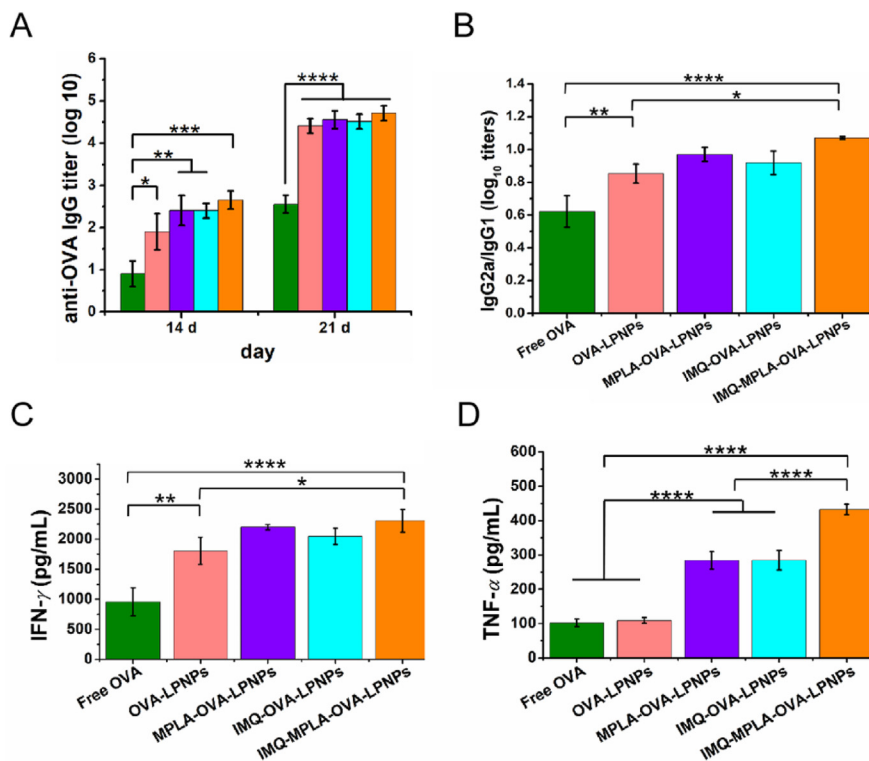


Figure 9 (A) Antigen-specific IgG titers and (B) Ratio of IgG2a/IgG1 in the serum of immunized mice; (C) IFN- γ and (D) TNF- α production of splenocytes from immunized mice. Data are presented as mean \pm SD ($n = 3$). * $P < 0.05$, ** $P < 0.01$, *** $P < 0.001$ and **** $P < 0.0001$ vs. indicated.

greatly promoted the percentage by 4.2- and 6.0-fold, respectively. In addition, IMQ-MPLA-OVA-LPNPs with dual agonists elicited significantly higher levels of CD86 than LPNPs-based nanovaccines without or with only one agonist. The MHC I expression on DCs immunized with IMQ-MPLA-OVA-LPNPs was also significantly greater than other groups except for MPLA-OVA-LPNPs. In comparison to IMQ-OVA-LPNPs with TLR7 agonist, MPLA-OVA-LPNPs with TLR4 agonist were more efficient in activating DCs, especially significantly promoting CD86 expression. This was probably due to that MPLA was incorporated within the lipid layer of the MPLA-OVA-LPNPs, thus it can be directly recognized by the TLR4, which is present on the surface of the DCs. The interaction of MPLA and TLR4 facilitated the internalization of MPLA-OVA-LPNPs and subsequently activated DCs *via* TLR4 signaling pathway. However, for IMQ-OVA-LPNPs, the hydrophobic IMQ was encapsulated in the hydrophobic polymer core. After uptake by DCs, only when the IMQ was released in the endosome, can it ligate with TLR7 which was expressed within endosomal compartment to activate DCs *via* TLR7 signaling pathway. Taken together, these results indicated that LPNPs-based nanovaccines promoted DCs maturation in draining LNs and IMQ-MPLA-OVA-LPNPs with spatio-temporal delivery of both intra- and extracellular TLR agonists was most effective probably due to the synergistic effect of multiple TLRs in activating DCs *via* triggering different signaling pathways.

3.5. *In vivo* immunization results

To assess the effect of LPNPs-based nanovaccines on cellular immune response, the mice were vaccinated two times with

different samples and then the splenocytes were obtained and stimulated with OVA. After that, the resulted cells were labeled by fluorescent antibodies against CD3, CD8, CD4, CD19, CD69, SIINFEKL-MHC I, CD44, CD62L and measured using flow cytometry (BD).

First, OVA-specific CD4⁺ and CD8⁺ T cells were measured to evaluate the generation degree of antigen-specific T cells in mice vaccinated with various preparations. As shown in Fig. 6, OVA-LPNPs induced more efficient proliferation of CD4⁺ and CD8⁺ T cells than Free OVA did. Greater T cell proliferation was observed in mice immunized with IMQ-OVA-LPNPs and MPLA-OVA-LPNPs as compared to OVA-LPNPs. More importantly, IMQ-MPLA-OVA-LPNPs with dual adjuvants further enhanced CD4⁺ and CD8⁺ T cell proliferation.

Then, the expression of CD69, a surface marker of T- and B-lymphocyte activity was analyzed to assess the activation of effector immune cells⁴⁹. OVA-LPNPs triggered significantly higher CD69 than Free OVA did, indicating the efficient activation of B cells, CD4⁺ and CD8⁺ T cells after encapsulation of OVA in the LPNPs (Fig. 7A–C). MPLA-OVA-LPNPs further upregulated the CD69 expression on CD4⁺ T cells and B cells compared to OVA-LPNPs. Moreover, in comparison to OVA-LPNPs with only one adjuvant, IMQ-MPLA-OVA-LPNPs with dual adjuvants significantly enhanced the CD69 expression on B cells. The CD69 expression on CD4⁺ and CD8⁺ T cells was also significantly elevated by IMQ-MPLA-OVA-LPNPs compared to IMQ-OVA-LPNPs.

Next, antigen-specific CD8⁺ T cell response was detected through staining re-stimulated splenocytes by SIINFEKL-MHC I (H-2Kb) pentamer. It was found that all OVA-loaded DOTAP-LPNPs with adjuvant were able to elicit higher OVA-specific

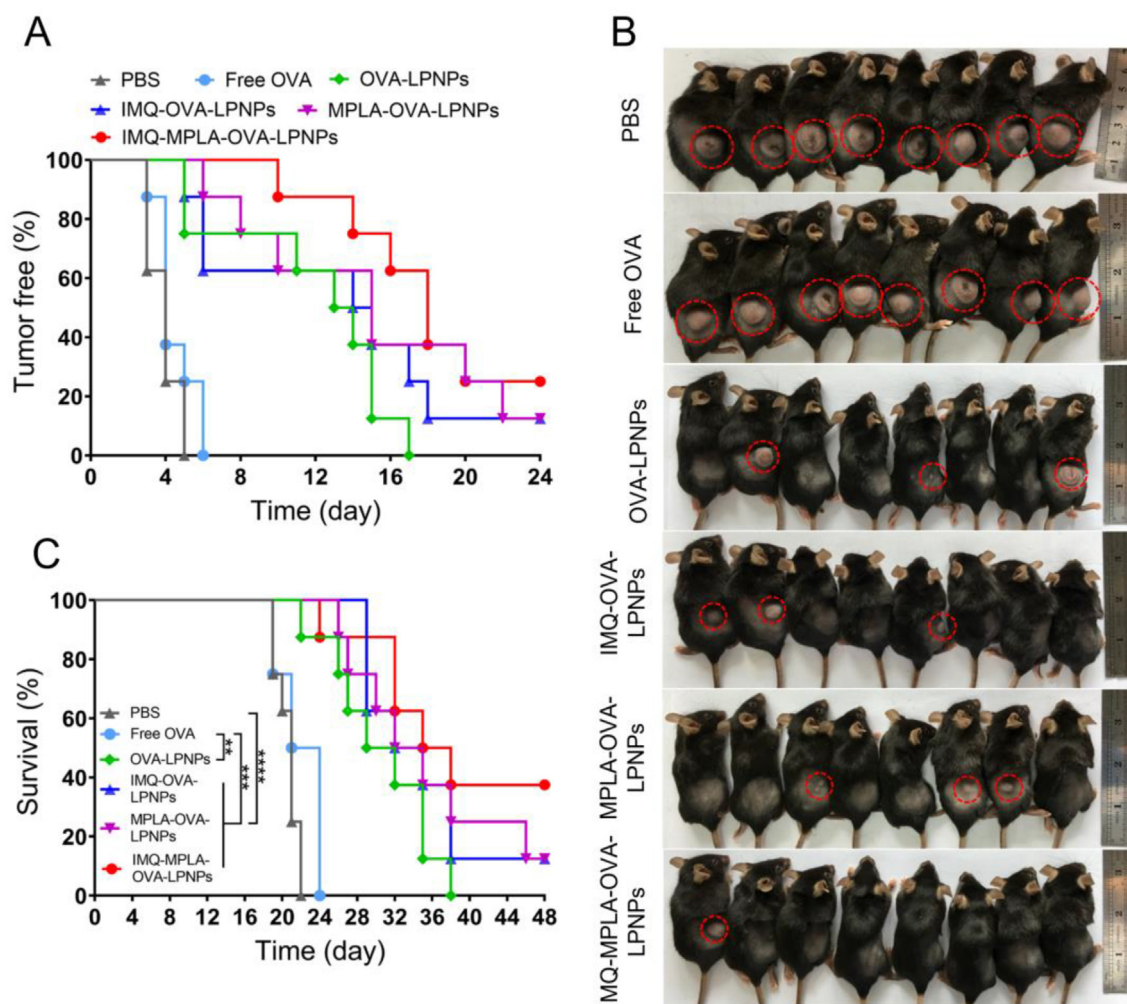


Figure 10 Prophylactic effect of various LPNPs-based nanovaccines against EG7-OVA tumor occurrence and growth *in vivo*. (A) Percent tumor-free mice and (B) photograph of vaccinated mice (Day 12) after tumor challenge. (C) Survival curves of EG7-OVA tumor bearing mice. Data are presented as mean \pm SD ($n = 8$). $**P < 0.01$, $***P < 0.001$ and $****P < 0.0001$ vs. indicated.

CD8⁺ T cells than Free OVA control and OVA-LPNPs without adjuvant (Fig. 7D). MPLA-OVA-LPNPs induced higher immune responses than IMQ-OVA-LPNPs, while IMQ-MPLA-OVA-LPNPs exhibited the greatest frequency of antigen-specific CD8⁺ T cells among all the OVA-loaded DOTAP-LPNPs.

The eventual aim of a vaccine is to generate long-term immunological memory, which can quickly engender robust humoral and cellular immune responses when encountering the pathogens and result in preventing reinfection or reducing the severity of disease⁵⁰. Memory T lymphocytes can be distinguished as effector memory (T_{EM}) and central memory (T_{CM}) cells. The T_{EM} elicits immediate effector T cells (T helper cells for CD4⁺ and CTLs for CD8⁺), while T_{CM} cells guarantee long-term protection⁵¹. In the present study, T_{CM} marker (CD44^{hi}CD62L^{hi}) and T_{EM} marker (CD44^{hi}CD62L^{low}) were determined by FACS (BD) to evaluate the memory T cell responses. As shown in Fig. 8, OVA-LPNPs exhibited significantly greater T_{EM} of CD4⁺ and CD8⁺ T cells than Free OVA. MPLA-OVA-LPNPs further significantly increased the percentage of T_{EM} in CD4⁺ and CD8⁺ T cells as well as T_{CM} in CD4⁺ T cells than OVA-LPNPs without immunostimulant and IMQ-OVA-LPNPs

with TLR7 agonist. The different TLR4 and TLR7 localization on DCs, the spatio-temporal delivery of MPLA and IMQ *via* LPNPs, as well as the sustained release of IMQ within the endosomal compartment led to the results that MPLA-OVA-LPNPs achieved a higher level of T cell immune memory than IMQ-OVA-LPNPs did. More importantly, IMQ-MPLA-OVA-NPs with dual immunostimulants generated the highest T_{CM} and T_{EM} of CD4⁺ and CD8⁺ T cells, demonstrating the strongest T cell memory responses.

3.6. The effect of LPNPs-based nanovaccines on antigen-specific antibody responses and cytokine secretion in mice

The effect of LPNPs-based nanovaccines on inducing humoral immune response was evaluated *in vivo*. C57BL/6 mice were subcutaneously injected with Free OVA or various OVA-loaded DOTAP-LPNPs twice at a 2-week interval, and anti-OVA antibodies were determined by ELISA on Days 7, 14, and 21 post first immunization. On Day 7, the anti-OVA IgG titers of all samples were below detection limit. On Day 14, although all groups showed low titers, LPNPs-based vaccines produced significantly

higher anti-OVA IgG titers than Free OVA did (Fig. 9A). On Day 21 (7 days post-boost), the anti-OVA IgG titers of all groups augmented dramatically but the differences among them still existed. Anti-OVA IgG titers (log 10) of mice immunized with OVA-LPNPs, MPLA-OVA-LPNPs, IMQ-OVA-LPNPs and IMQ-MPLA-OVA-LPNPs increased to 4.41, 4.56, 4.51, and 4.71, respectively, which were significantly higher than that of treated with Free OVA (2.56). This result demonstrated that TLR stimulation can increase the magnitude of antibody responses, which was in consistent with previous reports²⁴. Then, the IgG isotypes were analyzed to evaluate the effect of LPNPs-based nanovaccines on eliciting Th1 or Th2 biased humoral immune response. IgG2a isotype is associated with a Th1 response, while Th2 response promotes the production of IgG1 isotype⁵². As shown in Fig. 9B, the LPNPs-based vaccines elevated a higher ratio of IgG2a/IgG1 than Free OVA and IMQ-MPLA-OVA-LPNPs elicited the highest IgG2a to IgG1 ratio, indicating that encapsulating OVA and TLR agonists facilitated anti-OVA specific Th1 polarization. In addition, IFN- γ , a typical Th1 cytokine, was also promoted by 1.89–2.41-fold in mice treated with LPNPs-based nanovaccines compared with Free OVA (Fig. 9C). The elevated IFN- γ secretion further confirmed the activation of T cell-dependent immune responses⁵³. Moreover, TNF- α , a cell-derived inflammatory cytokine with powerful antitumoral activity, was significantly augmented by LPNPs-based nanovaccines in comparison to Free OVA (Fig. 9D). IMQ-OVA-LPNPs and MPLA-OVA-LPNPs with single immunostimulant were more efficient in promoting TNF- α than OVA-LPNPs, while IMQ-MPLA-OVA-LPNPs with dual immunostimulants further significantly elevated TNF- α production. The above results confirmed the good capacity of LPNPs-based nanovaccines especially IMQ-MPLA-OVA-LPNPs with dual immunostimulants for inducing Th1-skewed humoral and cellular immune responses.

3.7. Preventive effect of LPNPs-based nanovaccines on EG7-OVA tumor occurring

To evaluate the prophylactic effect of various LPNPs-based nanovaccines, C57BL/6 mice were intradermally immunized by various formulations twice with a 2-week interval. 7 days post the second immunization, the mice were challenged subcutaneously with 1×10^6 EG7-OVA tumor cells and the tumor growth was monitored. As depicted in Fig. 10A, palpable tumors were observed on Day 6 on all the mice treated with Free OVA or PBS control, and then the tumor grew very rapidly. On Day 12, the tumor volume reached $590.8 \pm 236.6 \text{ mm}^3$ and $838.1 \pm 254.5 \text{ mm}^3$ for Free OVA and PBS treated mice, respectively, indicating that Free OVA had no protective effect on mice against EG7-OVA tumor challenge. In contrast, the tumor occurring was remarkably retarded by vaccination with the formulated nanovaccines. Fig. 10B showed that the percentages of tumor-free mice were 62.5% (5 of 8 mice) for OVA-LPNPs, IMQ-OVA-LPNPs and MPLA-OVA-LPNPs, and increased to 87.5% (7 of 8 mice) for IMQ-MPLA-OVA-NPs with dual immunomodulators on Day 12. On Day 24, all mice vaccinated with OVA-LPNPs developed tumor, whereas one out of eight mice treated with IMQ-OVA-NPs and MPLA-OVA-NPs remained tumor free. More importantly, the nanovaccines with dual immunomodulators were the most effective, since two out of eight mice did not develop tumor at the end of the experiment (Day 48). Survival analysis demonstrated that mice treated with nanovaccines significantly prolonged survival compared to the

mice immunized with PBS or Free OVA (Fig. 10C). Moreover, the nanovaccines with both MPLA and IMQ immunomodulators further increased survival efficacy, exhibiting the longest survival with a median survival time of 37 days.

4. Conclusions

In the present study, LPNPs-based nanovaccines composed of cationic DOTAP lipid and PCL-PEG-PCL copolymer have been successfully fabricated for programmed co-delivery of model antigen OVA, and dual-agonists (MPLA and IMQ) to the same DCs. The IMQ-MPLA-OVA-LPNPs nanovaccines with dual-agonists can synergistically stimulate intracellular TLR7 *via* IMQ and extracellular TLR4 *via* MPLA, showing excellent capability to promote DCs maturation both *in vitro* and *in vivo*. Furthermore, LPNPs-based nanovaccines enhanced internalization into DCs and migration to draining LNs, which contributed to antigen cross-presentation and specific T-cell activation, then induced robust antigen-specific CD8⁺ T cell response and Th1-biased antibody responses, achieved long-lived T-cell memory. Upon prophylactic vaccination, IMQ-MPLA-OVA-LPNPs efficiently inhibited tumor growth and greatly increased survival efficacy. Taking together, the formulated LPNPs-based nanovaccines offer an effective approach to simultaneously deliver antigen and dual-agonists in a spatio-temporal manner and hold considerable potential as prophylactic vaccine in cancer immunotherapy. Further, ablative therapeutic drugs such as radiosensitizers, chemotherapeutics, and photosensitizers can be loaded into LPNPs simultaneously to promote the *in-situ* release of TAAs to achieve personalized prevention and treatment of cancer or infectious diseases.

Acknowledgments

This work was financially supported by National Natural Science Foundation of China (82072059 and 82172090), CAMS Innovation Fund for Medical Sciences (CIFMS, 2021-I2M-1-058, China), Fundamental Research Funds for the Central Universities (2019PT320028 and 2019-0831-03, China), Tianjin Municipal Natural Science Foundation (20JCYBJC00030, China).

Author contributions

Dunwan Zhu and Linhua Zhang conceived and designed the research. Nannan Wang and Yueyue Zuo carried out the experiments and performed data analysis. Shengjie Wu participated part of the experiments. Chenlu Huang revised the manuscript. All of the authors have read and approved the final manuscript.

Conflicts of interest

The authors declare no conflicts of interest.

References

1. Chen G, Yang YY, Xu Q, Ling MJ, Lin HM, Ma W, et al. Self-amplification of tumor oxidative stress with degradable metallic complexes for synergistic cascade tumor therapy. *Nano Lett* 2020;20:8141–50.

2. Yang YY, Liu X, Ma W, Xu Q, Chen G, Wang YF, et al. Light-activatable liposomes for repetitive on-demand drug release and immunopotentiality in hypoxic tumor therapy. *Biomaterials* 2021;**265**: 120456.
3. Fitzmaurice C, Abate D, Abbasi N, Abbastabar H, Abd-Allah F, Abdel-Rahman O, et al. Global, regional, and national cancer incidence, mortality, years of life lost, years lived with disability, and disability-adjusted life-years for 29 cancer groups, 1990 to 2017: a systematic analysis for the global burden of disease study. *JAMA Oncol* 2019;**5**:1749–68.
4. Xie Q, Ding J, Chen Y. Role of CD8⁺ T lymphocyte cells: Interplay with stromal cells in tumor microenvironment. *Acta Pharm Sin B* 2021;**11**:1365–78.
5. Zheng P, Ding BB, Jiang ZY, Xu WG, Li G, Ding JX, et al. Ultrasound-augmented mitochondrial calcium ion overload by calcium nanomodulator to induce immunogenic cell death. *Nano Lett* 2021;**21**: 2088–93.
6. Hurwitz AA, Watkins SK. Immune suppression in the tumor microenvironment: a role for dendritic cell-mediated tolerization of T cells. *Cancer Immunol Immunother* 2012;**61**:289–93.
7. Mildner A, Jung S. Development and function of dendritic cell subsets. *Immunity* 2014;**40**:642–56.
8. Lizée G, Basha G, Tiong J, Julien JP, Tian MM, Biron KE, et al. Control of dendritic cell cross-presentation by the major histocompatibility complex class I cytoplasmic domain. *Nat Immunol* 2003;**4**: 1065–73.
9. Yu L, Wang ZJ, Mo ZM, Zou BH, Yang YY, Sun R, et al. Synergetic delivery of triptolide and Ce6 with light-activatable liposomes for efficient hepatocellular carcinoma therapy. *Acta Pharm Sin B* 2021;**11**: 2004–15.
10. Sun YJ, Feng XR, Wan C, Lovell JF, Jin HL, Ding JX. Role of nanoparticle-mediated immunogenic cell death in cancer immunotherapy. *Asian J Pharm Sci* 2021;**16**:129–32.
11. Liu JH, Li ZM, Zhao DY, Feng XR, Wang CX, Li D, et al. Immunogenic cell death-inducing chemotherapeutic nanoformulations potentiate combination chemioimmunotherapy. *Mater Des* 2021;**202**: 109465.
12. Islam MA, Rice J, Reesor E, Zope H, Tao W, Lim M, et al. Adjuvant-pulsed mRNA vaccine nanoparticle for immunoprophylactic and therapeutic tumor suppression in mice. *Biomaterials* 2021;**266**: 120431.
13. Zhu GZ, Zhang FW, Ni QQ, Niu G, Chen XY. Efficient nanovaccine delivery in cancer immunotherapy. *ACS Nano* 2017;**11**: 2387–92.
14. Yang YY, Yu YJ, Chen H, Meng XX, Ma W, Yu M, et al. Illuminating platinum transportation while maximizing therapeutic efficacy by gold nanoclusters via simultaneous near-infrared-I/II imaging and glutathione scavenging. *ACS Nano* 2020;**14**:13536–47.
15. Feng XR, Xu WG, Li ZM, Song WT, Ding JX, Chen XS. Immunomodulatory nanosystems. *Adv Sci* 2019;**6**:1900101.
16. Sheng KC, Kalkanidis M, Pouniotis DS, Esparon S, Tang CK, Apostolopoulos V, et al. Delivery of antigen using a novel mannoseylated dendrimer potentiates immunogenicity *in vitro* and *in vivo*. *Eur J Immunol* 2008;**38**:424–36.
17. Xiao Q, Li X, Li Y, Wu ZF, Xu CJ, Chen ZJ, et al. Biological drug and drug delivery-mediated immunotherapy. *Acta Pharm Sin B* 2021;**11**: 941–60.
18. Moon JJ, Suh H, Bershteyn A, Stephan MT, Liu HP, Huang B, et al. Interbilayer-crosslinked multilamellar vesicles as synthetic vaccines for potent humoral and cellular immune responses. *Nat Mater* 2011;**10**:243–51.
19. Mandal B, Bhattacharjee H, Mittal N, Sah H, Balabathula P, Thoma LA, et al. Core-shell-type lipid-polymer hybrid nanoparticles as a drug delivery platform. *Nanomedicine* 2013;**9**:474–91.
20. Scott EA, Stano A, Gillard M, Maio-Liu AC, Swartz MA, Hubbell JA. Dendritic cell activation and T cell priming with adjuvant- and antigen-loaded oxidation-sensitive polymersomes. *Biomaterials* 2012;**33**:6211–9.
21. Beaudette TT, Bachelder EM, Cohen JA, Obermeyer AC, Broaders KE, Fréchet MJM, et al. *In vivo* studies on the effect of co-encapsulation of CpG DNA and antigen in acid-degradable micro-particle vaccines. *Mol Pharm* 2009;**6**:1160–9.
22. Schlosser E, Mueller M, Fischer S, Basta S, Busch DH, Gander B, et al. TLR ligands and antigen need to be coencapsulated into the same biodegradable microsphere for the generation of potent cytotoxic T lymphocyte responses. *Vaccine* 2008;**26**:1626–37.
23. Wilson JT, Keller S, Manganiello MJ, Cheng C, Lee CC, Opara C, et al. pH-Responsive nanoparticle vaccines for dual-delivery of antigens and immunostimulatory oligonucleotides. *ACS Nano* 2013;**7**: 3912–25.
24. Kasturi SP, Skountzou I, Albrecht RA, Koutsonanos D, Hua T, Nakaya HI, et al. Programming the magnitude and persistence of antibody responses with innate immunity. *Nature* 2011;**470**:543–7.
25. Mata-Haro V, Cekic C, Martin M, Chilton PM, Casella CR, Mitchell TC. The vaccine adjuvant monophosphoryl lipid A as a TRIF-biased agonist of TLR4. *Science* 2007;**316**:1628–32.
26. Schülke S, Vogel L, Junker AC, Hanschmann KM, Flaczyk A, Vieths S, et al. A fusion protein consisting of the vaccine adjuvant monophosphoryl lipid A and the allergen ovalbumin boosts allergen-specific Th1, Th2, and Th17 responses *in vitro*. *J Immunol Res* 2016;**2016**:4156456.
27. Ismaili J, Rennesson J, Aksoy E, Vekemans J, Vincart B, Amraoui Z, et al. Monophosphoryl lipid A activates both human dendritic cells and T cells. *J Immunol* 2002;**168**:926–32.
28. Bohannon JK, Hernandez A, Enkhbaatar P, Adams WL, Sherwood ER. The immunobiology of toll-like receptor 4 agonists: from endotoxin tolerance to immunoadjuvants. *Shock* 2013;**40**: 451–62.
29. Siefert AL, Caplan MJ, Fahmy TM. Artificial bacterial biomimetic nanoparticles synergize pathogen-associated molecular patterns for vaccine efficacy. *Biomaterials* 2016;**97**:85–96.
30. Primard C, Poecheim J, Heuking S, Sublet E, Esmaeili F, Borchard G. Multifunctional PLGA-based nanoparticles encapsulating simultaneously hydrophilic antigen and hydrophobic immunomodulator for mucosal immunization. *Mol Pharm* 2013;**10**:2996–3004.
31. Vicente S, Peleteiro M, Díaz-Freitas B, Sanchez A, González-Fernández Á, Alonso MJ. Co-delivery of viral proteins and a TLR7 agonist from polysaccharide nanocapsules: a needle-free vaccination strategy. *J Control Release* 2013;**172**:773–81.
32. Stanley MA. Imiquimod and the imidazoquinolones: mechanism of action and therapeutic potential. *Clin Exp Dermatol* 2002;**27**:571–7.
33. Brubaker SW, Bonham KS, Zaroni I, Kagan JC. Innate immune pattern recognition: a cell biological perspective. *Annu Rev Immunol* 2015;**33**:257–90.
34. Bocanegra Gondan AI, Ruiz-de-Angulo A, Zabaleta A, Gómez Blanco N, Cobaleda-Siles BM, García-Granda MJ, et al. Effective cancer immunotherapy in mice by polyIC-imiquimod complexes and engineered magnetic nanoparticles. *Biomaterials* 2018;**170**:95–115.
35. Ma YF, Zhuang Y, Xie XF, Wang C, Wang F, Zhou DM, et al. The role of surface charge density in cationic liposome-promoted dendritic cell maturation and vaccine-induced immune responses. *Nanoscale* 2011;**3**:2307–14.
36. Zhang LH, He YN, Ma GL, Song CX, Sun HF. Paclitaxel-loaded polymeric micelles based on poly(ϵ -caprolactone)-poly(ethylene glycol)-poly(ϵ -caprolactone) triblock copolymers: *in vitro* and *in vivo* evaluation. *Nanomedicine* 2012;**8**:925–34.
37. Hu CY, Chen Z, Wu SJ, Han YF, Wang H, Sun HF, et al. Micelle or polymersome formation by PCL-PEG-PCL copolymers as drug delivery systems. *Chin Chem Lett* 2017;**28**:1905–9.
38. Zhang LH, Zhu DW, Dong X, Sun HF, Song CX, Wang C, et al. Folate-modified lipid-polymer hybrid nanoparticles for targeted paclitaxel delivery. *Int J Nanomed* 2015;**10**:2101–14.
39. Huang CL, Zhang LH, Guo Q, Zuo YY, Wang NN, Wang H, et al. Robust nanovaccine based on polydopamine-coated mesoporous silica nanoparticles for effective photothermal-immunotherapy against melanoma. *Adv Funct Mater* 2021;**31**:2010637.

40. Kanamala M, Wilson WR, Yang M, Palmer BD, Wu ZM. Mechanisms and biomaterials in pH-responsive tumour targeted drug delivery: a review. *Biomaterials* 2016;**85**:152–67.
41. Gao J, Ochyl LJ, Yang E, Moon JJ. Cationic liposomes promote antigen cross-presentation in dendritic cells by alkalizing the lysosomal pH and limiting the degradation of antigens. *Int J Nanomed* 2017;**12**:1251–64.
42. Seo N, Akiyoshi K, Shiku H. Exosome-mediated regulation of tumor immunology. *Cancer Sci* 2018;**109**:2998–3004.
43. Kim J, Li WA, Choi Y, Lewin SA, Verbeke CS, Dranoff G, et al. Injectable, spontaneously assembling, inorganic scaffolds modulate immune cells *in vivo* and increase vaccine efficacy. *Nat Biotechnol* 2015;**33**:64–72.
44. Du YQ, Xia YF, Zou YJ, Hu YN, Fu JQ, Wu J, et al. Exploiting the lymph-node-amplifying effect for potent systemic and gastrointestinal immune responses *via* polymer/lipid nanoparticles. *ACS Nano* 2019;**13**:13809–17.
45. Li AW, Sobral MC, Badrinath S, Choi Y, Graveline A, Stafford AG, et al. A facile approach to enhance antigen response for personalized cancer vaccination. *Nat Mater* 2018;**17**:528–34.
46. Zeng Q, Li HM, Jiang H, Yu J, Wang Y, Ke H, et al. Tailoring polymeric hybrid micelles with lymph node targeting ability to improve the potency of cancer vaccines. *Biomaterials* 2017;**122**:105–13.
47. Jiang H, Wang Q, Sun X. Lymph node targeting strategies to improve vaccination efficacy. *J Control Release* 2017;**267**:47–56.
48. Pan C, Wu J, Qing S, Zhang X, Zhang LL, Yue H, et al. Biosynthesis of self-assembled proteinaceous nanoparticles for vaccination. *Adv Mater* 2020;**32**:e2002940.
49. Cibrián D, Sánchez-Madrid F. CD69: from activation marker to metabolic gatekeeper. *Eur J Immunol* 2017;**47**:946–53.
50. Wang C, Liu P, Zhuang Y, Li P, Jiang BL, Pan H, et al. Lymphatic-targeted cationic liposomes: a robust vaccine adjuvant for promoting long-term immunological memory. *Vaccine* 2014;**32**:5475–83.
51. Youngblood B, Hale JS, Ahmed R. T-cell memory differentiation: insights from transcriptional signatures and epigenetics. *Immunology* 2013;**139**:277–84.
52. Xia YF, Wu J, Wei W, Du YQ, Wan T, Ma XW, et al. Exploiting the pliability and lateral mobility of Pickering emulsion for enhanced vaccination. *Nat Mater* 2018;**17**:187–94.
53. Feng XR, Xu WG, Liu JH, Li D, Li G, Ding JX, et al. Polypeptide nanoformulation-induced immunogenic cell death and remission of immunosuppression for enhanced chemioimmunotherapy. *Sci Bull* 2021;**66**:362–73.